sciendo

PROCEEDINGS OF THE LATVIAN ACADEMY OF SCIENCES. Section B,
Vol. 74 (2020), No. 6 (729), pp. 396–403.

DOI: 10.2478/prolas-2020-0058

OXYGEN EVOLUTION REACTION ON A N-DOPED $CO_{0.5}$-TERMINATED CO_3O_4 (001) SURFACE

Gulbanu A. Kaptagay[1,#], Nazira A. Sandibaeva[1], Talgat M. Inerbaev[2, 3], Yuri A. Mastrikov[4], Eugene A. Kotomin[4]

[1] Kazakh National Women's Teacher Training University, Almaty 050000, KAZAKHSTAN

[2] Sobolev Institute of Geology and Mineralogy, Siberian Branch of the Russian Academy of Sciences, Novosibirsk 630090, RUSSIA

[3] L. N. Gumilyov Eurasian National University, Nur-Sultan 010000, KAZAKHSTAN

[4] Institute of Solid State Physics, University of Latvia, 8 Ķengaraga Str., Rīga, LV-1063, LATVIA

[#] Corresponding author, gulbanu.kaptagai@mail.ru

Contributed by Eugene A. Kotomin

Recent experimental findings suggest that the catalytic activity of Co_3O_4 for oxygen evolution reaction (OER) could be improved by nitrogen doping. We present preliminary OER modelling on a N-doped Co_3O_4 surface, with varying concentration of the dopant and its spatial distribution around Co_{oct} and Co_{tet} adsorption sites. The overpotential was calculated for two adsorption sites on seven types of N-doped Co_3O_4 surface. The largest calculated overpotential value for a N-doped surface was ~1V.

Key words: *Cobalt oxide, OER, electrocatalyst, first principles calculations.*

INTRODUCTION

Oxygen Evolution Reaction (OER) takes place in many electrochemical devices for renewable energy production (Cook *et al*., 2010), including catalysts for water splitting (Hu *et al*., 2019). The overall performance of this reaction considerably depends on the *overpotential* η (Bard and Faulkner, 2002); a lower overpotential is associated with a higher reaction rate. High OER performance was demonstrated by noble metal oxides — Ru- and IrO_2 (Reier *et al*., 2012). One of the cheaper alternatives of noble metal oxides with a relatively low overpotential is Co_3O_4 (Zasada *et al*., 2010; Chen and Selloni, 2012; Liu *et al*., 2017). Many studies suggest that oxide catalyst overpotential can be lowered by doping (Ohnishi *et al*., 2007; García-Mota *et al*., 2011; Liao *et al*., 2012; Bothra and Pati, 2016; Wang *et al*., 2018). It was experimentally found that N-doping is beneficial for OER on a Co_3O_4 surface (Xu *et al*., 2017). Other studies (Wang *et al*., 2019) reported similar results (Table 1).

Earlier computational studies revealed that N_o is stable in the Co_3O_4 bulk (Kaptagay *et al*., 2018) as well as on a $Co_{0.5}$-terminated (001) surface (Kaptagay *et al*., 2020). Exploiting the models developed in these studies, we simulated OER on a N-doped Co_3O_4 surface.

Table 1. OER on undoped and doped Co_3O_4 surfaces — surface orientation, overpotential, Process Determining Step (PDS)

Material	Surface orientation	η, V	PDS	Study
Co_3O_4	(110)	0.76		Bothra and Pati, 2016
$Co_{2.75}Cu_{0.25}O_4$	(110)	0.41		Bothra and Pati, 2016
Co_3O_4		1.79**		Xu *et al*., 2017
N-doped Co_3O_4 nanosheet with V_O		1.54**		Xu *et al*., 2017
Co_3O_4	(110)	0.64	O*	Wang *et al*., 2019
N-doped Co_3O_4	(110)	0.41	OOH*	Wang *et al*., 2019

* adsorbed species; ** to reach the current density of 10 mA cm^{-2}

METHOD AND MODEL

Co_3O_4 has a structure of a normal spinel, symmetry group 227 (Anonymous, 2020). The tetragonal 8*a* sites are occupied by Co^{2+}, and the octahedral 16*d* sites by Co^{3+}. O^{2-} ions occupy 32*e* sites.

A N-doped $Co_{0.5}$-terminated (001) Co_3O_4 surface was modelled by a 11-plane stoichiometric symmetric slab, as de-

scribed in (Kaptagay *et al.*, 2020), containing ten formula units. The structure of Co_3O_4 comprised alternating Co_{tet} and $Co_{oct\ 2}\ O_4$ planes. Removing half of Co_{tet} atoms from the plane gave rise to a $Co_{0.5}$ plane. The structure of the undoped slab was fully relaxed. The symmetry of the slab was preserved, making adsorption on both terminating planes completely equivalent. Four concentrations of nitrogen in the terminating plane were tested — 12.5, 25, 50, and 100%. For each concentration smaller that 100%, two distributions of the dopant were designed (Kaptagay *et al.*, 2020). A schematic view of the $Co_{0.5}$-terminated (001) Co_3O_4 slab is given in Figure 1. Each doped surface was defined as a set of substituted numbered oxygen atoms N_O. For doped slabs, as well as for adsorption configurations, only atomic positions were optimised. Initial adsorption configurations were set based on the results of previous study (Kaptagay *et al.*, 2015).

The whole water splitting reaction with oxygen production can be presented as four elementary reaction steps, as suggested by Norskov (Valdés *et al.*, 2008):

$$\text{Step 1: } H_2O + {}^* \rightarrow OH^* + H^+ + e^- \quad (1)$$

$$\text{Step 2: } OH^* \rightarrow O^* + H^+ + e^- \quad (2)$$

$$\text{Step 3: } H_2O + O^* \rightarrow OOH^* + H^+ + e^- \quad (3)$$

$$\text{Step 4: } OOH^* \rightarrow O_2 + {}^* + H^+ + e^-, \quad (4)$$

where * denotes adsorbed species or the surface itself.

The Gibbs free energies are calculated as

$$\Delta G_i = \Delta E_i + \Delta ZPE_i\text{-}T\Delta S_i, \quad (5)$$

where ΔE_i is the adsorption energy, calculated by means of DFT method, ΔZPE_i – Zero Point Energy, T – temperature and ΔS_i entropy of the corresponding i step of the reaction.

ΔE_i is calculated with respect to combinations of H_2O(l) and H_2(g).

$$\Delta E_{OH^*} = E(OH^*) - (E(^*) + [E(H_2O) - 1/2E(H_2)]); \quad (6)$$

$$\Delta E_{O^*} = E(O^*) - (E(^*) + [E(H_2O)) - E(H_2)]); \quad (7)$$

$$\Delta E_{OOH^*} = E(OOH^*) - (E(^*) + [2E(H_2O) - 3/2E(H_2)]), \quad (8)$$

where * denotes adsorbed species or the surface itself.

ZPE values and $T\Delta S_i$ taken from (Liu *et al.*, 2017) (Table 2).

Overpotential η was calculated according to the standard relation:

$$\eta^{OVER} = \max\ [\Delta G_i] / e\text{–}1.23[V], \quad (9)$$

where 1.23 V is the standard potential for water molecule dissociation.

The details of the thermodynamic model are given in (Kaptagay *et al.*, 2015).

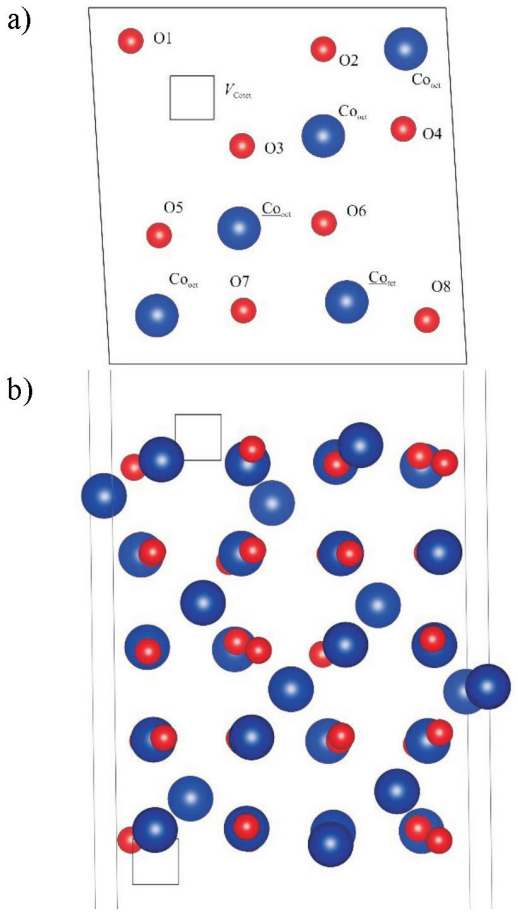

Fig. 1. Top (a) and side (b) view of the the $Co_{0.5}$-terminated (001) Co_3O_4 slab. Co $_{oct}$ and Co $_{tet}$ adsorption sites are underlined. Co $_{tet}$ is the only atom in the topmost plane. The presence of $V_{Co\ tet}$ vacancy in the terminating plane makes this termination $Co_{0.5}$.

Table 2. Zero-Point Energy corrections and entropic contributions to free energies

	ZPE, eV	$T\Delta S_i$, eV
H_2O (l)	0.56	0.67 (0.035 bar)
H_2 (g)	0.27	0.41
OH^*	0.36	0
O^*	0.07	0
OOH^*	0.45	0

* adsorbed species.

Computational details. Full structural optimisation was performed by the Density Functional Theory (DFT) (Kohn and Sham, 1965) method as implemented in the computer code VASP (Kresse and Furthmüller, 1996). This code is widely used for the atomic and electronic structure calculations of solids from first principles. Core electrons were substituted with Ultra Soft (US) potentials with the Projector Augmented Wave (PAW) method (Kresse and Joubert, 1999). Computational parameters were carefully tested in previous computational studies on the N-doped Co_3O_4 bulk (Kaptagay *et al.*, 2018) and surface (Kaptagay *et al.*, 2020). Exchange-correlation was described by the PBE functional (Perdew *et al.*, 1996). The Hubbard correction $U - J = 3$ eV

(Dudarev *et al*., 1998) was applied to *d*-electrons of Co_{tet} as well as Co_{oct} atoms. Spin-polarisation was implemented in the *A*-type AntiFerromagnetic (AAF) order, alternating on the Co_{tet} planes. Although the particular magnetic order is not significant for the process under study, taking spin-polarisation into account is essential for obtaining the proper oxidation state of Co_{tet} cations. The Brillouin zone (Brillouin, 1930) was sampled with the 4x4x2 Monkhorst-Pack scheme (Monkhorst and Pack, 1976). The plane-wave basis set has a kinetic energy cut-off of 550 eV. Charge redistribution was analysed by the Bader method, as implemented by Henkelman *et al*. (2006), Yu and Trinkle (2011).

RESULTS

The OER intermediates, OH, O and OOH, were placed atop the two most catalytically active adsorption sites — Co_{oct} and Co_{tet} (Fig. 2) on both terminating planes (Xu *et al*., 2019).

Note that only the molecular adsorption mode was considered in the present study. In (Zasada *et al*., 2010) the dissociative mode of H_2O adsorption on Co_3O_4 (001) was found more preferable. The Co-O bond length of 1.81 Å for a OH fragment of H_2O from (Zasada *et al*., 2010) can be compared to the same Co-O bond for a single OH (Table 3). The configurational differences were minimised to reveal the energetic ones. However, for OOH adsorption, the configurational difference was noticeable: there was variation in length of the O–O bond and hydrogen bond with either one or both oxygen atoms.

The energetics of OER was considered at three applied potentials — $U = 0$, standard –1.23V, and U for the max ΔG_i. DFT adsorption energies and Gibbs free energy change ΔG_i were calculated for each reaction step (Fig. 3).

García-Mota *et al*. (2012) suggested that the trends in activity between oxide materials are to the first approximation determined by the O* binding energy. For many systems, a zero overpotential value was obtained, which can be attributed to structural peculiarities of the adsorbed OOH (Table 4).

A strong correlation between ΔE_{OOH*} and ΔE_{OH*} was found previously (Man *et al*., 2011). For OER, on many oxides the difference between two energies is 3.20 eV. For a perfect catalyst this difference should be 2.44 eV. These two values served as reference lines for the obtained data (Fig. 4).

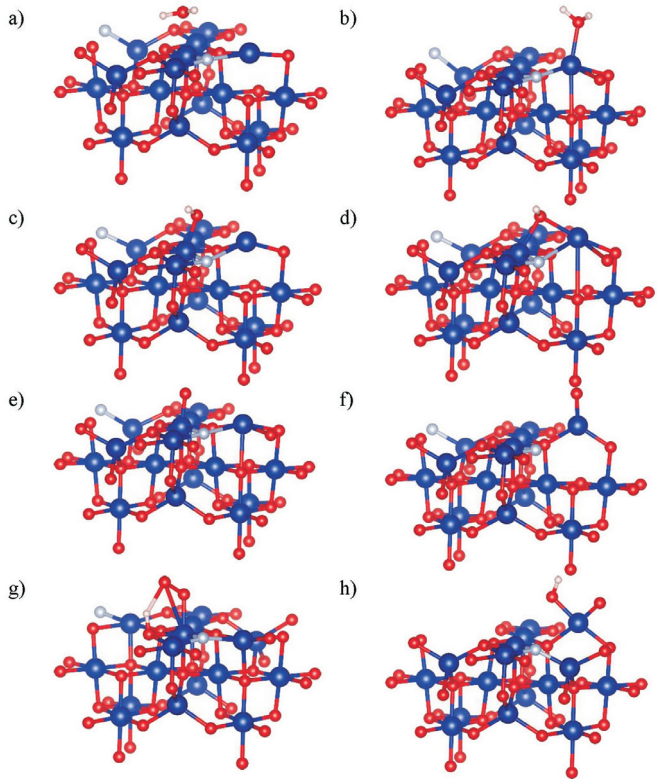

Fig. 2. Lateral view of H_2O (a,b). OH (c,d), O (e,f) and OOH (g,h). adsorbed on a N-doped (12.5% of No in plane, position #7 in Figure 1 a) $Co_{0.5}$-terminated Co_3O_4 (001) surface atop Co_{oct} (a,c,e,g) and Co_{tet}(b,d,f,h) adsorption sites.

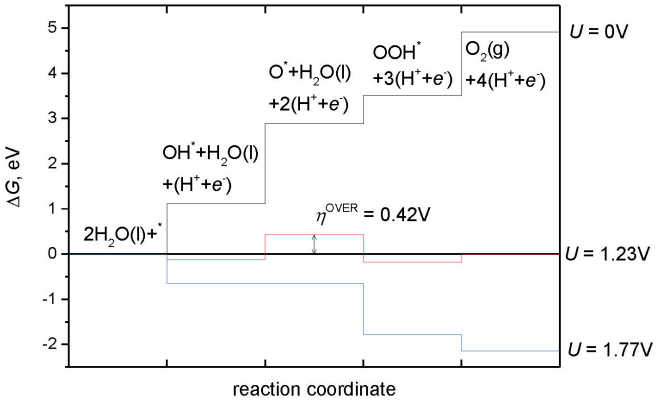

Fig. 3. The Gibbs free energy diagram for OER on an undoped $Co_{0.5}$-terminated (001) Co_3O_4 surface at the Co_{oct} adsorption site for $U = 0$, 1.23 and 1.77 V. At $U = 1.77$ V all steps were thermodynamically accessible. The overpotential corresponds to the step with the highest ΔG value – 1.77eV.

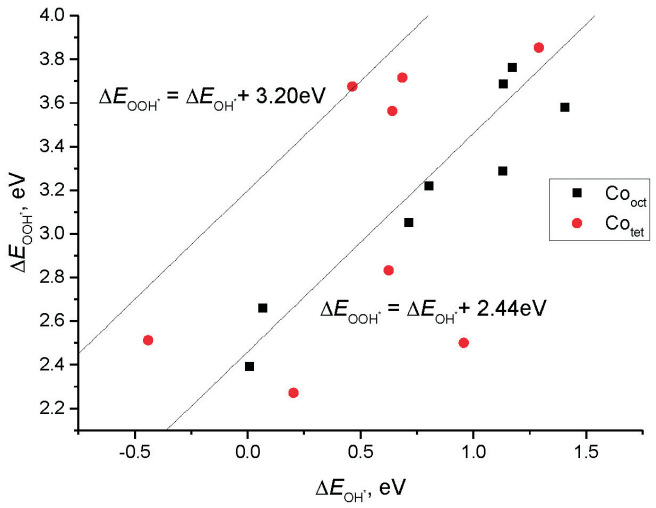

Fig. 4. Adsorption energies ΔE_{OOH*} (ΔE_{OH*}) for Co_{oct} and Co_{tet} adsorption sites.

Table 3. Interatomic distances in Å and atomic charges in *e* of H_2O, OH, O and OOH on a $Co_{0.5}$-terminated (001) Co_3O_4 surface. Atomic charge is given for the Co atom of the adsorption site and oxygen atom of H_2O dissociation products. N_O are placed according to the numbering of O atoms in Figure 1

Surface	0% N									
ads. site	Co_{oct}									
	distance, Å							charge, *e*		
step	O-Co	O-Co	H-Co	H-Co	O-H	O-H	O-O	Co	O	O
H_2O	2.04		2.27	2.34	0.99	0.98		1.45	–1.93	
OH	1.80		2.26		0.98			1.60	–1.40	
O	1.63							1.63	–0.52	
OOH	1.87	2.72	2.29		1.65		1.32	1.45	–0.30	–0.26
ads. site	Co_{tet}									
	distance, Å							charge, *e*		
step	O-Co	O-Co	H-Co	H-Co	O-H	O-H	O-O	Co	O	O
H_2O	2.06		2.78	2.67	0.97	0.97		1.32	–1.95	
OH	1.76		2.34		0.96			1.35	–1.53	
O	1.64							1.35	–0.67	
OOH	1.63	1.79	2.31		0.98		2.51	1.47	–0.58	–1.41
surface	12.5% N: 6									
ads. site	Co_{oct}									
	distance, Å							charge, *e*		
step	O-Co	O-Co	H-Co	H-Co	O-H	O-H	O-O	Co	O	O
H_2O	2.03		2.27	2.31	0.99	0.99		1.44	–1.92	
OH	1.79		2.25		0.98			1.57	–1.38	
O	1.62							1.58	–0.51	
OOH	1.97	2.78	2.38			1.83	1.29	1.49	–0.23	–0.18
ads. site	Co_{tet}									
	distance, Å							charge, *e*		
step	O-Co	O-Co	H-Co	H-Co	O-H	O-H	O-O	Co	O	O
H_2O	2.10		2.65	2.60	0.97	0.98		1.23	–1.94	
OH	2.01		2.57		0.98			1.23	–1.54	
O	1.61							1.33	–0.59	
OOH	1.64	1.80	2.31		0.98		2.54	1.43	–0.59	–1.42
surface	12.5% N: 7									
ads. site	Co_{oct}									
	distance, Å							charge, *e*		
step	O-Co	O-Co	H-Co	H-Co	O-H	O-H	O-O	Co	O	O
H_2O	2.07		2.45	2.27	0.98	0.99		1.45	-1.92	
OH	1.83		2.34		0.98			1.55	-1.44	
O	1.64							1.59	-0.53	
OOH	1.91	2.75	2.34		1.80		1.30	1.43	-0.25	-0.20
ads. site	Co_{tet}									
	distance, Å							charge, *e*		
step	O-Co	O-Co	H-Co	H-Co	O-H	O-H	O-O	Co	O	O
H_2O	2.13		2.75	2.65	0.97	0.98		1.33	–1.95	
OH	2.07		2.68		0.98			1.57	–1.39	
O	1.64							1.35	–0.69	
OOH	1.68	1.79	2.33		0.98		2.53	1.41	–0.57	–1.43
surface	25% N: 6,8									
ads. site	Co_{oct}									
	distance, Å							charge, *e*		
step	O-Co	O-Co	H-Co	H-Co	O-H	O-H	O-O	Co	O	O
H_2O	2.04		2.27	2.32	0.99	0.99		1.53	–1.91	
OH	1.79		2.26		0.98			1.57	–1.39	
O	1.63							1.59	–0.56	
OOH	1.93	2.76	2.37		1.75		1.30	1.51	–0.26	–0.20
ads. site	Co_{tet}									
	distance, Å							charge, *e*		
step	O-Co	O-Co	H-Co	H-Co	O-H	O-H	O-O	Co	O	O
H_2O	2.15		2.73	2.63	0.98	0.98		1.25	–1.95	
OH	1.95		2.52		0.98			1.19	–1.52	
O	1.64							1.32		–0.56
OOH	1.65	1.81	2.32		0.98		2.60	1.39	–0.61	–1.44

Table 3. (Continued)

surface	25% N: 2,7									
ads. site	Co_{oct}									
	distance, Å							charge, *e*		
step	O-Co	O-Co	H-Co	H-Co	O-H	O-H	O-O	Co	O	O
H_2O	2.05		2.42	2.28	0.98	0.99		1.44	–1.92	
OH	1.82		2.32		0.98			1.57	–1.43	
O	1.63							1.59	–0.53	
OOH	1.91	2.75	2.31		1.70		1.31	1.43	–0.27	–0.22
ads. site	Co_{tet}									
	distance, Å							charge, *e*		
step	O-Co	O-Co	H-Co	H-Co	O-H	O-H	O-O	Co	O	O
H_2O	2.16		2.75	2.62	0.97	0.98		1.31	–1.95	
OH	1.77		2.49		0.97			1.28	–1.57	
O	1.64							1.35	–0.71	
OOH	1.63	1.80	2.32		0.98		2.53	1.47	–0.60	–1.42
surface	50% N: 3,5-7									
ads. site	Co_{oct}									
step	distance, Å							charge, *e*		
	O-Co	O-Co	H-Co	H-Co	O-H	O-H	O-O	Co	O	O
H_2O	2.39		2.67	2.70	0.98	0.98		1.37	–1.97	
OH	1.85		2.35		0.98			1.36	–1.46	
O	1.65							1.40	–0.58	
OOH	2.02	2.88	2.39		2.11		1.28	1.37	–0.22	–0.13
ads. site	Co_{tet}									
	distance, Å							charge, *e*		
step	O-Co	O-Co	H-Co	H-Co	O-H	O-H	O-O	Co	O	O
H_2O	2.15		2.72	2.61	0.98	0.98		1.24	–1.95	
OH	1.95		2.53		0.98			1.23	–1.55	
O	1.61							1.33	–0.63	
OOH	1.64	1.80	2.30		0.98		2.53	1.44	–0.61	–1.42
surface	50% N: 2,6-8									
ads. site	Co_{oct}									
	distance, Å							charge, *e*		
step	O-Co	O-Co	H-Co	H-Co	O-H	O-H	O-O	Co	O	O
H_2O	2.05		2.42	2.34	0.98	0.99		1.42	–1.91	
OH	1.82		2.32		0.98			1.52	–1.44	
O	1.64							1.51	–0.56	
OOH	1.97	2.78	2.44		1.89		1.29	1.41	–0.24	–0.18
ads. site	Co_{tet}									
	distance, Å							charge, *e*		
step	O-Co	O-Co	H-Co	H-Co	O-H	O-H	O-O	Co	O	O
H_2O	2.16		2.76	2.63	0.97	0.98		1.19	–1.95	
OH	1.75		2.31		0.98			1.31	–1.42	
O	1.60							1.31	–0.57	
OOH	1.64	1.82	2.33		0.98		2.59	1.40	–0.60	–1.46
surface	100% N: 1-8									
ads. site	Co_{oct}									
	distance, Å							charge, *e*		
step	O-Co	O-Co	H-Co	H-Co	O-H	O-H	O-O	Co	O	O
H_2O	2.09		2.38	2.46	0.99	0.98		1.33	–1.94	
OH	1.83		2.33		0.98			1.39	–1.44	
O	1.63							1.43	–0.55	
OOH	1.98	2.85	2.40		2.07		1.28	1.34	–0.23	–0.15
ads. site	Co_{tet}									
	distance, Å							charge, *e*		
step	O-Co	O-Co	H-Co	H-Co	O-H	O-H	O-O	Co	O	O
H_2O	2.14		2.80	2.70	0.97	0.98		1.19	–1.96	
OH	2.09		2.71		0.98			1.19	–1.55	
O	1.60							1.24	–0.60	
OOH	1.64	1.81	2.31		0.98		2.55	1.39	–0.61	–1.43

Table 4. Calculated with respect to H_2O and H_2 binding energies, and Gibbs free energies in eV at U = 0, 1.23V and at U for the max ΔG_i. The value of overpotential η^{OVER} is **bold underlined** in V

Surface	0% N									
ads. site	Co_{oct}					Co_{tet}				
step	DFT adsorption energy, eV	ΔG, eV	U = 0.00	U = 1.23	U = 1.77	DFT adsorption energy, eV	ΔG, eV	U = 0.00	U = 1.23	U = 1.96
OH	0.71	1.11	1.11	-0.12	–0.65	0.96	1.36	1.36	0.13	–0.60
O	2.84	1.77	2.88	**0.42**	–0.65	2.61	1.29	2.65	0.19	–1.27
OOH	3.05	0.63	3.51	-0.18	–1.79	2.50	0.31	2.96	–0.73	–2.92
O_2(g)		1.41	4.92	0.00	–2.15		1.96	4.92	**0.00**	–2.92
surface	12.5% N: 6									
ads. site	Co_{oct}					Co_{tet}				
step	DFT adsorption energy, eV	ΔG, eV	U = 0.00	U = 1.23	U = 2.07	DFT adsorption energy, eV	ΔG, eV	U = 0.00	U = 1.23	U = 2.19
OH	0.01	0.41	0.41	–0.82	–1.66	0.20	0.60	0.60	–0.63	–1.59
O	2.16	1.79	2.20	–0.26	–1.94	1.68	1.12	1.72	–0.74	–2.66
OOH	2.39	0.65	2.85	–0.84	–3.35	2.27	1.01	2.73	–0.96	–3.84
O_2(g)		2.07	4.92	**0.00**	–3.35		2.19	4.92	**0.00**	–3.84
surface	12.5% N: 7									
ads. site	Co_{oct}					Co_{tet}				
step	DFT adsorption energy, eV	ΔG, eV	U = 0.00	U = 1.23	U = 1.76	DFT adsorption energy, eV	ΔG, eV	U = 0.00	U = 1.23	U = 2.21
OH	0.80	1.20	1.20	–0.03	–0.56	0.46	0.86	0.86	–0.37	–1.35
O	2.92	1.76	2.96	**0.50**	–0.56	1.88	1.06	1.92	–0.54	–2.50
OOH	3.22	0.71	3.68	–0.01	–1.60	3.68	2.21	4.14	**0.45**	–2.50
O_2(g)		1.24	4.92	0.00	–2.12		0.78	4.92	0.00	–3.93
surface	25% N: 6,8									
ads. site	Co_{oct}					Co_{tet}				
step	DFT adsorption energy, eV	ΔG, eV	U = 0.00	U = 1.23	U = 1.68	DFT adsorption energy, eV	ΔG, eV	U = 0.00	U = 1.23	U = 1.85
OH	1.17	1.57	1.57	0.34	–0.10	0.64	1.04	1.04	–0.19	–0.81
O	3.21	1.68	3.25	**0.79**	–0.10	2.13	1.13	2.17	–0.29	–1.54
OOH	3.76	0.97	4.22	0.53	–0.81	3.56	1.85	4.02	**0.33**	–1.54
O_2(g)		0.70	4.92	0.00	–1.78		0.90	4.92	0.00	–2.50
surface	25% N: 2,7									
ads. site	Co_{oct}					Co_{tet}				
step	DFT adsorption energy, eV	ΔG, eV	U = 0.00	U = 1.23	U = 2.03	DFT adsorption energy, eV	ΔG, eV	U = 0.00	U = 1.23	U = 1.95
OH	0.07	0.47	0.47	–0.76	–1.57	–0.44	–0.04	–0.04	–1.27	–1.99
O	2.46	2.03	2.50	**0.04**	–1.57	1.38	1.46	1.42	–1.04	–2.47
OOH	2.66	0.62	3.12	–0.57	–2.98	2.51	1.55	2.97	–0.72	–2.87
O_2(g)		1.80	4.92	0.00	–3.21		1.95	4.92	**0.00**	–2.87
surface	50% N: 3,5-7									
ads. site	Co_{oct}					Co_{tet}				
step	DFT adsorption energy, eV	ΔG, eV	U = 0.00	U = 1.23	U = 1.61	DFT adsorption energy, eV	ΔG, eV	U = 0.00	U = 1.23	U = 1.63
OH	1.13	1.53	1.53	0.30	–0.08	0.63	1.03	1.03	–0.20	–0.60
O	3.10	1.61	3.14	**0.68**	–0.08	1.79	0.80	1.83	–0.63	–1.43
OOH	3.29	0.61	3.75	0.06	–1.08	2.83	1.46	3.29	–0.40	–1.59
O_2(g)		1.17	4.92	0.00	–1.51		1.63	4.92	**0.00**	–1.59
surface	50% N: 2,6-8									
ads. site	Co_{oct}					Co_{tet}				
step	DFT adsorption energy, eV	ΔG, eV	U = 0.00	U = 1.23	U = 1.95	DFT adsorption energy, eV	ΔG, eV	U = 0.00	U = 1.23	U = 1.77
OH	1.13	1.53	1.53	0.30	–0.40	0.69	1.09	1.09	–0.14	–0.68
O	3.43	1.94	3.47	**1.01**	–0.40	2.37	1.33	2.41	–0.05	–1.12
OOH	3.69	0.68	4.15	0.46	–1.66	3.72	1.77	4.18	**0.49**	–1.12
O_2(g)		0.77	4.92	0.00	–2.83		0.74	4.92	0.00	–2.14
surface	100% N: 1-8									
ads. site	Co_{oct}					Co_{tet}				
step	DFT adsorption energy, eV	ΔG, eV	U = 0.00	U = 1.23	U = 1.81	DFT adsorption energy, eV	ΔG, eV	U = 0.00	U = 1.23	U = 2.10
OH	1.41	1.81	1.81	**0.58**	0.00	1.29	1.69	1.69	0.46	–0.41
O	3.04	1.28	3.08	0.62	–0.53	2.17	0.52	2.21	–0.25	–2.00
OOH	3.58	0.96	4.04	0.35	–1.38	3.85	2.10	4.31	**0.62**	–2.00
O_2(g)		0.88	4.92	0.00	–2.30		0.61	4.92	0.00	–3.49

Table 5. Overpotential η^{OVER} in V, calculated with ΔE_{OOH} (as in Table 3) and $\Delta E_{OOH} = \Delta E_{OH}$+3.2eV. For the underscored values the potential determining step remained the same, for the values in **bold** the value of overpotential remained the same as well

N concentration in plane	substituted O atoms	ΔE_{OOH}		$\Delta E_{OOH} = \Delta E_{OH} + 3.2$eV	
		Co_{oct}	Co_{tet}	Co_{oct}	Co_{tet}
0.0	-	**0.42**	0.00	**0.42**	0.93
12.5	6	0.00	0.00	-0.26	0.17
12.5	7	**0.50**	**0.45**	**0.50**	**0.43**
25.0	6,8	**0.79**	0.33	**0.79**	0.61
25.0	2.7	**0.04**	0.00	**0.04**	-0.47
50.0	3.5–7	0.68	0.00	1.10	0.60
50.0	2.6–8	**1.01**	0.49	**1.01**	0.66
100.0	1–8	0.58	0.62	1.38	1.26

Structural instabilities of adsorbed OOH can be eliminated by replacement of ΔE_{OOH} DFT energies with ΔE_{OH} + 3.2eV. For nine types of surface, the PDS remained the same, and for six of them even the value of overpotential η^{OVER} did not change (Table 5). This comparison shows that adsorption of OOH atop Co_{oct} was much more structurally stable than atop Co_{tet}, and therefore the calculated values of overpotential were more consistent.

CONCLUSIONS

The highest overpotential value for the examined N-doped surface was ~1 V, which makes OER reaction on this Co_3O_4 (001) surface possible at a reasonable rate and material doping promising for improvement of the water splitting efficiency. For OER on 25% N_O (2.7) concentration atop Co_{oct}, the overpotential was lowered by 0.38 V, with respect to an undoped surface.

The obtained statistical data showed a high sensitivity of Gibbs free energy as well as overpotential on computational details. The main source of energetic diversity was most likely caused by configurational instability of OOH adsorption, illustrated in Figure 2. Artificially eliminating this instability, we verified calculated values of overpotential.

The performed calculations created a large amount of data for the future interpretation and comparison. The designed configurations can also be used as a solid platform for OER modelling on spinel-like materials.

ACKNOWLEDGEMENTS

The project AP05131211 "First principles investigation on catalytic properties of N-doped Co_3O_4." was funded by the Ministry of Education and Science of the Republic of Kazakhstan.

The work was partly supported by COST (European Cooperation in Science and Technology) Action 18234 (YM and EK). The work of T. Inerbaev was performed under the state assignment of Sobolev Institute of Geology and Mineralogy Siberian Branch of the Russian Academy of Sciences. YM and EK thank Sun-to-Chem project of ERA-Net.

REFERENCES

Anonymous (2020). Co3O4 Crystal Structure – SpringerMaterials. Available at: https://materials.springer.com/isp/crystallographic/docs/sd_0311005 (accessed 11.12.20).

Bard, A. J., Faulkner, L. R. (2002). Allen J. Bard and Larry R. Faulkner. Electrochemical Methods: Fundamentals and Applications, New York: Wiley, 2001, 2nd ed. *Russ. J. Electrochem*., **38**, 1364–1365.

Bothra, P., Pati, S. K. (2016). Activity of water oxidation on pure and (Fe, Ni, and Cu)-substituted Co3O4. *ACS Energy Lett.*, **1**, 858–862.

Brillouin, L. (1930). Les électrons libres dans les métaux et le role des réflexions de Bragg. *J. Phys. Radium*, **1**, 377–400.

Chen, J., Selloni, A. (2012). Water adsorption and oxidation at the Co_3O_4 (110) surface. *J. Phys. Chem. Lett*., **3**, 2808–2814.

Cook, T. R., Dogutan, D. K., Reece, S. Y., Surendranath, Y., Teets, T. S., Nocera, D. G. (2010). Solar energy supply and storage for the legacy and nonlegacy worlds. *Chem. Rev*., **110**, 6474–6502.

Dudarev, S. L., Botton, G. A., Savrasov, S. Y., Humphreys, C. J., Sutton, A. P. (1998). Electron-energy-loss spectra and the structural stability of nickel oxide: An LSDA+U study. *Phys. Rev. B*, **57**, 1505–1509.

García-Mota, M., Bajdich, M., Viswanathan, V., Vojvodic, A., Bell, A. T., Nørskov, J. K. (2012). Importance of correlation in determining electrocatalytic oxygen evolution activity on cobalt oxides. *J. Phys. Chem. C*, **116**, 21077–21082.

García-Mota, M., Vojvodic, A., Metiu, H., Man, I. C., Su, H. Y., Rossmeisl, J., Nørskov, J. K. (2011). Tailoring the activity for oxygen evolution electrocatalysis on rutile TiO_2(110) by transition-metal substitution. *Chem. Cat. Chem*., **3**, 1607–1611.

Henkelman, G., Arnaldsson, A., Jónsson, H. (2006). A fast and robust algorithm for Bader decomposition of charge density. *Comput. Materi. Sci*., **36**, 354–360.

Hu, C., Zhang, L., Gong, J. (2019). Recent progress made in the mechanism comprehension and design of electrocatalysts for alkaline water splitting. *Energy Environ. Sci*., **12**, 2620–2645.

Kaptagay, G. A., Inerbaev, T. M., Akilbekov, A. T., Koilyk, N. O., Abuova, A. U., Sandibaeva, N. A. (2020). First principles modelling of the N-doped Co<inf>0.5</inf> -terminated (0 0 1) Co<inf>3</inf>O<inf>4</inf> surface. *Nucl. Instrum. Meth. Phys. Res. Section B*, **465**, 11–14.

Kaptagay, G. A. A., Inerbaev, T. M. M., Mastrikov, Yu. A., Kotomin, E. A. A., Akilbekov, A. T. T. (2015). Water interaction with perfect and fluorine-doped Co<inf>3</inf>O<inf>4</inf> (100) surface. *Solid State Ionics*, **277**, 77–82.

Kaptagay, G. A. A., Mastrikov, Y. A. A., Kotomin, E. A. A. (2018). First-principles modelling of N-doped Co<inf>3</inf>O<inf>4</inf>. *Latv. J. Phys. Techn. Sci*., **55**, 36–42.

Kohn, W., Sham, L. J. (1965). Self-consistent equations including exchange and correlation effects. *Phys. Rev*., **140**, A1133–A1138.

Kresse, G., Furthmüller, J. (1996). Efficiency of ab-initio total energy calculations for metals and semiconductors using a plane-wave basis set. *Comput. Mater. Sci*., **6**, 15–50.

Kresse, G., Joubert, D. (1999). From ultrasoft pseudopotentials to the projector augmented-wave method. *Phys. Rev. B*, **59**, 1758–1775.

Liao, P., Keith, J. A., Carter, E. A. (2012). Water oxidation on pure and doped hematite (0001) surfaces: Prediction of Co and Ni as effective dopants for electrocatalysis. *J. Amer. Chem. Soc*., **134**, 13296–13309.

Liu, L., Jiang, Z., Fang, L., Xu, H., Zhang, H., Gu, X., Wang, Y. (2017). Probing the crystal plane effect of Co_3O_4 for enhanced electrocatalytic per-

formance toward efficient overall water splitting. *ACS Appl. Mater. Interfaces*, **9**, 27736–27744.

Man, I. C., Su, H. Y., Calle-Vallejo, F., Hansen, H. A., Martínez, J. I., Inoglu, N. G., Kitchin, J., Jaramillo, T. F., Nørskov, J. K., Rossmeisl, J. (2011). Universality in oxygen evolution electrocatalysis on oxide surfaces. *Chem. Cat. Chem*., **3**, 1159–1165.

Monkhorst, H. J., Pack, J. D. (1976). Special points for Brillouin-zone integrations. *Phys. Rev. B*., **13**, 5188–5192.

Ohnishi, C., Asano, K., Iwamoto, S., Chikama, K., Inoue, M. (2007). Alkali-doped Co3O4 catalysts for direct decomposition of N_2O in the presence of oxygen. *Catalysis Today,* **120**, 145–150.

Perdew, J. P., Burke, K., Ernzerhof, M. (1996). Generalized gradient approximation made simple. *Phys. Rev. Lett*., **77**, 3865–3868.

Reier, T., Oezaslan, M., Strasser, P. (2012). Electrocatalytic oxygen evolution reaction (OER) on Ru, Ir, and Pt catalysts: A comparative study of nanoparticles and bulk materials. *ACS Catalysism,* **2**, 1765–1772.

Valdés, Á., Qu, Z. W., Kroes, G. J., Rossmeisl, J., Nørskov, J. K. (2008). Oxidation and photo-oxidation of water on TiO_2 surface. *J. Phys. Chem. C*, **112**, 9872–9879.

Wang, Z., Liu, H., Ge, R., Ren, X., Ren, J., Yang, D., Zhang, L., Sun, X. (2018). Phosphorus-doped Co_3O_4 nanowire array: A highly efficient bifunctional electrocatalyst for overall water splitting. *ACS Catalysis*, **8**, 2236–2241.

Wang, Z., Xu, W., Chen, X., Peng, Y., Song, Y., Lv, C., Liu, H., Sun, J., Yuan, D., Li, X., Guo, X., Yang, D., Zhang, L. (2019). Defect-rich nitrogen doped Co_3O_4 /C porous nanocubes Enable high-efficiency bifunctional oxygen electrocatalysis. *Adv. Funct. Mater*., **29**, 1902875.

Xu, L., Wang, Z., Wang, J., Xiao, Z., Huang, X., Liu, Z., Wang, S. (2017). N-doped nanoporous Co_3O_4 nanosheets with oxygen vacancies as oxygen evolving electrocatalysts. *Nanotechnology*, **28**, 165402.

Xu, Y., Zhang, F., Sheng, T., Ye, T., Yi, D., Yang, Y., Liu, S., Wang, X., Yao, J. (2019). Clarifying the controversial catalytic active sites of Co_3O_4 for the oxygen evolution reaction. *J. Mater. Chem. A*, **7**, 23191–23198.

Yu, M., Trinkle, D. R. (2011). Accurate and efficient algorithm for Bader charge integration. *J. Chem. Phys*., **134**, 064111.

Zasada, F., Piskorz, W., Cristol, S., Paul, J.-F., Kotarba, A., Sojka, Z. (2010). Periodic density functional theory and atomistic thermodynamic studies of cobalt spinel nanocrystals in wet environment: Molecular interpretation of water adsorption equilibria*. J. Phys. Chem. C*, **114**, 22245–22253.

Received 26 October 2020
Accepted in the final form 16 November 2020

SKĀBEKĻA EVOLŪCIJAS REAKCIJA UZ N-DOPĒTAS $CO_{0.5}$-TERMINĒTAS CO_3O_4 (001) VIRSMAS

Jaunākie eksperimentālie atklājumi liecina, ka Co_3O_4 katalītisko aktivitāti skābekļa evolūcijas reakcijai (OER) varētu uzlabot ar slāpekļa dopingu. Mēs iepazīstinām ar provizorisko OER modelēšanu uz N-leģētas Co_3O_4 virsmas, mainot dopanta koncentrāciju un tā telpisko sadalījumu ap Co_{oct} un Co_{tet} adsorbcijas vietām. Virspotenciāls tika aprēķināts divām adsorbcijas vietām uz septiņiem N-leģēta Co_3O_4 virsmas veidiem. Lielākā aprēķinātā virspotenciāla vērtība N-leģētai virsmai ir ~ 1V.